

Iron-Catalyzed Regiodivergent Hydrostannation of Alkynes: Intermediacy of Fe(IV)–H versus Fe(II)–Vinylidene

Jianguo Liu, Heng Song, Tianlin Wang, Jiong Jia, Qing-Xiao Tong,* Chen-Ho Tung, and Wenguang Wang*



Cite This: *J. Am. Chem. Soc.* 2021, 143, 409–419



Read Online

ACCESS |



Metrics & More

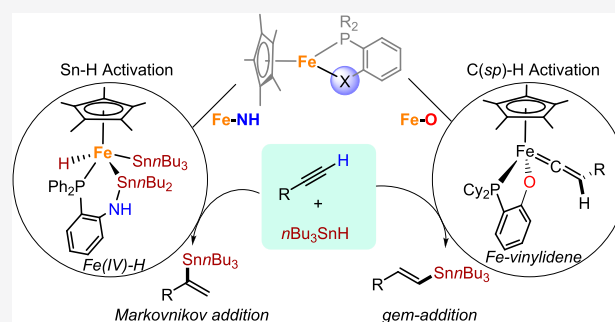


Article Recommendations



Supporting Information

ABSTRACT: We report an iron system, $\text{Cp}^*\text{Fe}(1,2\text{-R}_2\text{PC}_6\text{H}_4\text{X})$, which controls the Markovnikov and anti-Markovnikov hydrostannation of alkynes by tuning the ionic metal–heteroatom bonds (Fe–X) reactivity. The sequential addition of $n\text{Bu}_3\text{SnH}$ to the iron-amido catalyst (**1**, X = HN^- , R = Ph) affords a distanny Fe(IV)–H species responsible for syn-addition of the Sn–H bond across the $\text{C}\equiv\text{C}$ bond to produce branched α -vinylstannanes. Activation of the C(sp)–H bond of alkynes by an iron–aryloxide catalyst (**2**, X = O^- , R = Cy) affords an iron(II) vinylidene intermediate, allowing for gem-addition of the Sn–H to the terminal-carbon producing β -vinylstannanes. These catalytic reactions exhibit excellent regioselectivity and broad functional group compatibility and enable the large-scale synthesis of diverse vinylstannanes. Many new reactions have been established based on such a synthetic Fe–X platform to demonstrate that the initial step of the catalysis is conveniently controlled by the activation of either the tin hydride or the alkyne substrate.



INTRODUCTION

Transition-metal complexes featuring ionic metal–heteroatom bonds (M–X),¹ for example, imides,^{2,3} amides,^{4–8} thiolates,^{9–11} and alkoxides,^{12–14} are of particular interest in the exploration of metal–ligand cooperative catalysis. These M–X bonds are often highly polarized, allowing them to interact with either reagents or substrates in homogeneous catalysis or enzyme-catalyzed synthesis.^{15–17} In particular, metal-ligated strategies of this type promote the application of iron¹⁸ to process transformations under mild conditions. The chemistry involving the Fe–X bond provides not only mechanistic insight into the catalysis but also an opportunity to control the reaction selectivity and expand the catalytic strategy. Iron-catalyzed hydrometalation is emerging as an active field, and the Fe–X cooperative activation of B–H and Si–H bonds has attracted rapidly growing attention.¹⁹ In contrast, although hydrostannanes are useful metalloids, activation of the Sn–H bond by a synthetic iron system leading to hydrostannation has not been reported to date.

Vinylstannanes are practically useful synthetic intermediates that can couple with a wide range of electrophiles.²⁰ Stannylation of 1-alkynes with an $\text{R}_3\text{Sn–M}$ reagent (M = Sn, Si, B, Al, Mg) can reveal vinylstannanes upon subsequent protonolysis.²¹ Hydrostannation of alkynes with $\text{R}_3\text{Sn–H}$ is the most straightforward and atom-economic route to vinylstannanes.²² However, the control of $\text{R}_3\text{Sn–H}$ addition across alkynes is challenging. In particular, there is no

implemented general Markovnikov hydrostannation of both aromatic and aliphatic 1-alkynes since the first report on the α -stannylation of simple aliphatic alkynes with $n\text{Bu}_3\text{SnH}$.²³ Compared to B–H and Si–H bonds, the Sn–H bond is usually more likely to undergo homolytic cleavage, generating $\text{R}_3\text{Sn}\cdot$ and $\text{H}\cdot$ radicals. This complicates the outcome of the addition of a tin hydride to alkynes. Prior studies focused on regioselective hydrostannation using Pd,²⁴ Mo,²⁵ Ru,²⁶ Cu,^{21,27} and Mg catalysts.²⁸ However, the selective production of α - or β -vinylstannanes was often sensitive to steric or electronic factors. Although the oxidative addition of $\text{R}_3\text{Sn–H}$ (R = $n\text{Bu}$, Me, and Ph) was proposed for the Pd(0)-catalyzed hydrostannation,²⁹ the hydrostannation mechanism is probably the least understood metalloids–hydride addition to alkynes.^{22a} Exploring fundamental reactions between the transition-metal complex and $\text{R}_3\text{Sn–H}$ facilitates the development of general catalytic methods to control the reaction selectivity initially. Recently, it has been increasingly clear that the outcome of the reaction can be potentially controlled by using a well-defined catalyst, to tune the Sn–H bond activation mode. Fürstner et

Received: October 31, 2020

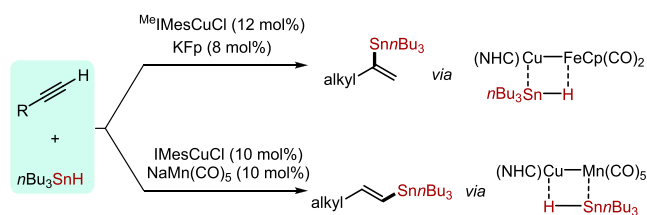
Published: December 29, 2020



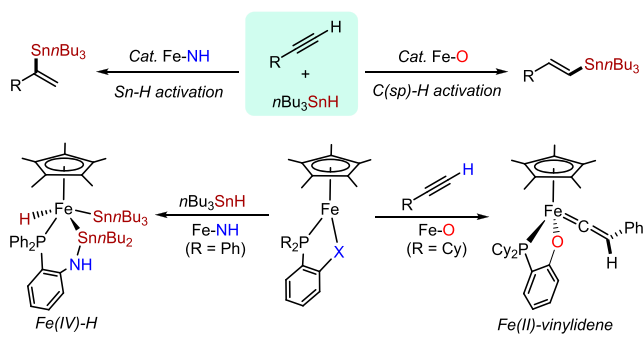
al. reported the $[\text{Cp}^*\text{RuCl}]$ -catalyzed hydrostannylation of functionalized internal alkynes^{26b} and proposed that this catalysis involved a σ -(H–Sn*n*Bu₃) intermediate, and the interaction between the chloride and protic functionality of the substrate dictates the regioselective hydrostannylation. Mankad et al. reported cooperative Sn–H activation by heterobimetallic (NHC)Cu–[M_{CO}] systems ([M_{CO}] = CpFe(CO)₂ or Mn(CO)₅) to generate Fe–H/Cu–Sn*n*Bu₃ or Cu–H/Mn–Sn*n*Bu₃ pairs that control the regioselective hydrostannylation of aliphatic 1-alkynes (Scheme 1a).³⁰ Oestreich and co-workers

Scheme 1. Cooperative Sn–H Activation for Alkyne Hydrostannylation

a) heterobimetallic cooperative Sn–H bond activation (Mankad, ref.30)



b) controlled activation of Sn–H and C(sp)–H bonds by Fe–X system (this work)



reported that the cooperative Ru–S reactivity of the Ohki–Tatsumi complexes enables the Sn–H bond to undergo heterolytic cleavage affording a stannylum ion-like tin electrophile together with Ru(II)–H species, which achieves the dehydrogenative stannylation of 1-alkynes.³¹

We planned to study the activating *n*Bu₃SnH reagent and the substrate, RC≡C–H,³² by tuning the Lewis acid–base coordination sphere interactions in the half-sandwich iron(II) system of Cp*Fe(1,2-R₂PC₆H₄X). The aim was to control the regioselectivity of catalytic alkyne hydrostannylation. We describe here the selective activation of *n*Bu₃SnH by an

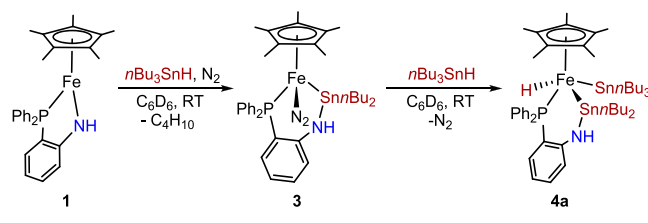
iron(II)–amido complex for the Markovnikov hydrostannylation of alkynes and the activation of 1-alkyne by iron(II)–aryloxide for the anti-Markovnikov hydrostannylation (Scheme 1b). Many new reactions have been established based on such a synthetic Fe–X platform to demonstrate the rational activating of the tin hydride and the alkyne for controlling the reaction selectivity.

RESULTS AND DISCUSSION

Synthesis and Characterization of Cp*Fe(1,2-R₂PC₆H₄X). Following the recently described procedure,¹¹ complexes **1** and **2** were prepared by treating $[\text{Cp}^*\text{Fe}(\text{NCMe})_3]\text{PF}_6$ in MeCN with a THF solution of 1,2-Ph₂PC₆H₄NHLi and 1,2-Cy₂PC₆H₄ONa, respectively. The ¹H NMR spectra of **1** and **2** in C₆D₆ show broadened and paramagnetically shifted signals between –64 and 37 ppm. The magnetic moments of **1** and **2** in solution were determined to be 2.52 and 3.21 μ_B, respectively, consistent with that reported for the intermediate-spin iron(II) complexes such as $[\text{Cp}^*\text{Fe}(1,2\text{-Ph}_2\text{PC}_6\text{H}_4\text{S})_2(\mu\text{-N}_2)]$ and Cp*Fe(NHC)Cl.^{11,33} The solid-state structures of **1** and **2** were confirmed by crystallographic analysis (Figure 1), which shows they are neutral five-coordination iron(II) half-sandwich compounds with a similar Cp*Fe(1,2-R₂PC₆H₄X) framework.

Activation of *n*Bu₃SnH by **1.** Changing the basic site (X) from amido to oxide and modifying the coordination sphere leads to Cp*Fe(1,2-R₂PC₆H₄X) with very different reactivity. Reflecting by the reactions with *n*Bu₃SnH, **1** can activate the Sn–H bond by stepwise reactions with two molecules of the tin hydride (Scheme 2), whereas **2** is inert toward the Sn–H bond activation.

Scheme 2. Stepwise Activation of *n*Bu₃SnH by Complex **1**



Adding 1 equiv of *n*Bu₃SnH to **1** in C₆D₆ caused the orange solution to turn deep red in a few minutes. A phosphorus resonance at δ 63.4 (*J*¹¹⁹_{Sn–P} = 636 Hz, *J*¹¹⁷_{Sn–P} = 608 Hz) appeared in the ³¹P NMR spectrum of the solution, together with a stannyl signal at δ 228.8 (*d*, *J*_{P–Sn} = 636 Hz) in the ¹¹⁹Sn NMR spectrum. No hydride signal was observed in the ¹H

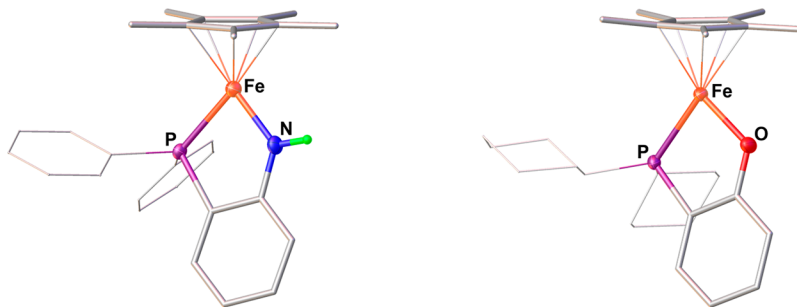


Figure 1. Solid-state structures of **1** (left) and **2** (right) with 50% probability thermal ellipsoids. For clarity, hydrogen atoms are omitted, and the two phenyl and cyclohexyl groups bonded at the phosphorus atom are drawn as lines. Selected bond distances (Å) and angles (deg): for **1**, Fe–P 2.203(1), Fe–N 1.842(3), P–Fe–N 84.6(1); for **2**, Fe–P 2.2409(6), Fe–O 1.900(1), P–Fe–O 86.94(5).

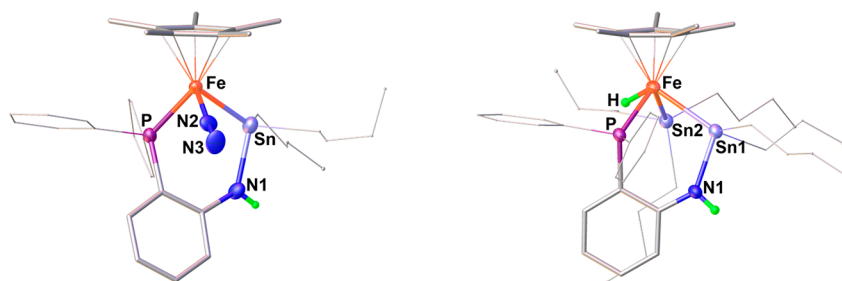


Figure 2. Structures of **3** (left) and **4a** (right) with 50% probability thermal ellipsoids. Selected bond distances (Å) and angles (deg): for **3** Fe–P 2.227(1), Fe–Sn 2.5002(6), N1–Sn 2.099(4), N2–N3 1.099(5), P–Fe–Sn 83.78(3), P–Fe–N2 89.9(1); for **4a** Fe–P 2.218 (2), Fe–Sn1 2.540(1), Fe–Sn2 2.666(1), Fe–H 1.28(5), Sn2–H 2.19(5), N–Sn1 2.108(5), P–Fe–Sn1 83.60(5), P–Fe–Sn2 104.52(5), Sn1–Fe–Sn2, 80.44(3).

NMR spectrum. Crystallographic analysis revealed the structure of a stannyl iron(II) dinitrogen compound, $\text{Cp}^*\text{Fe}(\text{N}_2)[1,2\text{-Ph}_2\text{PC}_6\text{H}_4\text{NH}(n\text{SnBu}_2)]$ (**3**, Figure 2). According to this structure, it appears that $n\text{Bu}_3\text{SnH}$ was activated by eliminating a butane molecule, and the rest of the $\text{Sn}n\text{Bu}_2$ motif was inserted into the Fe–N bond, forming an Fe–Sn bond. The production of butane gas was confirmed by GC analysis (Supporting Information, Figure S2). The N2–N3 separation is 1.099(5) Å, very close to 1.0977 Å for a free N_2 molecule.^{11a} In the IR spectrum of a toluene solution of **3**, the $\nu_{\text{N}=\text{N}}$ band was observed at 2064 cm^{-1} (Figure S19). These results suggest that the N_2 is weakly coordinated with the iron center and is replaceable. Indeed, after exposure of a Et_2O solution of **3** to a CO atmosphere, the dinitrogen ligand is substituted by CO, and this is accompanied by the appearance of a ν_{CO} band at 1906 cm^{-1} in the IR spectrum (Figure S25). The production of $\text{Cp}^*\text{Fe}(\text{CO})[1,2\text{-Ph}_2\text{PC}_6\text{H}_4\text{NH}(\text{Sn}n\text{Bu}_2)]$ was fully characterized by X-ray, NMR (^1H , ^{31}P , ^{119}Sn , and ^{13}C), and ESI-MS spectroscopy (Supporting Information).

$\text{Cp}(\text{CO})_2\text{FeSnR}_3$ (R = Bu, Ph) has been reported to be formed by the reaction of $[\text{CpFe}(\text{CO})_2]\text{Na}$ with ClSnR_3 .³⁴ Compounds of this sort can further react with HSiR_3 , HSnR_3 , or HGeR_3 upon photolysis, producing the iron(IV) hydride containing two group 14 element ligands.³⁵ These reactive features have attracted considerable attention to the photochemistry of $\text{Cp}_2\text{Fe}_2(\text{CO})_4$ or $\text{CpFe}(\text{CO})_2\text{L}$ with metallohydrides for the dehydrogenative dimerization of $t\text{Bu}_2\text{SnH}_2$ and hydrosilanes.³⁶ We found that **3** reacts readily with $n\text{Bu}_3\text{SnH}$ to afford a distannyl iron(IV) hydride complex (**4a**).

Treatment of **3** in d_8 -toluene with $n\text{Bu}_3\text{SnH}$ caused the red solution to turn brown. The ^{119}Sn NMR spectrum of **4a** displays two sets of doublets, one at δ 195.8 ($J_{\text{P-Sn}} = 634$ Hz) for the N-stabilized $n\text{Bu}_2\text{Sn}$ moiety and the other at δ 54.5 ($J_{\text{P-Sn}} = 126$ Hz) for the $n\text{Bu}_3\text{Sn}$ group. In the ^1H NMR spectrum, a characteristic hydride signal was observed at δ –12.3 (d, $J_{\text{P-H}} = 68$ Hz). The hydride resonance is flanked by tin satellites (Figure 3). The ^{31}P resonance is at δ 65.5 (s), only 2 ppm downfield from the parent complex (**3**).

Combined with the NMR spectra, crystallographic analysis established the structure of **4a** as a neutral complex with the formula $\text{Cp}^*\text{Fe}(\text{H})(\text{Sn}n\text{Bu}_3)[1,2\text{-Ph}_2\text{PC}_6\text{H}_4\text{NH}(\text{Sn}n\text{Bu}_2)]$ (Figure 2). The Fe–Sn($n\text{Bu}_3$) bond length of 2.666(1) Å is about 0.12 Å longer than the 2.540(1) Å observed in Fe–Sn($n\text{Bu}_2$). For comparison, the addition of $n\text{Bu}_3\text{SnH}$ to **3** causes the Fe–Sn($n\text{Bu}_2$) bond to increase only by 0.04 Å. These Fe–Sn bond distances all fall in the range of 2.50–2.67 Å reported for the stannyliron(IV) complexes.³⁷ The position of the hydride ligand was located and refined. The ($n\text{Bu}_3$)Sn–

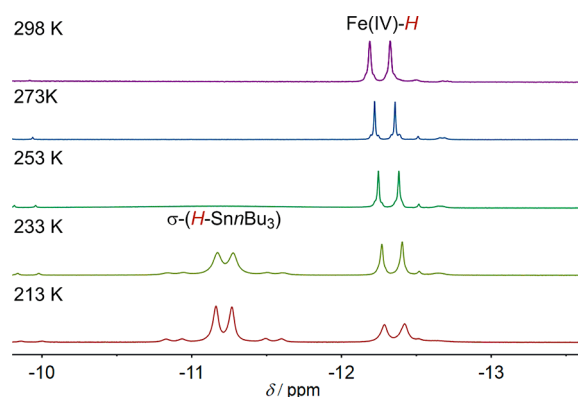
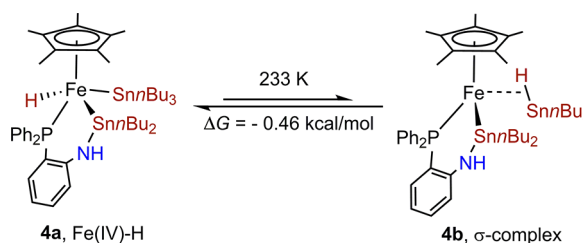


Figure 3. Variable-temperature ^1H NMR spectra of **4a** in d_8 -toluene.

H bond distance in **4a** is 2.19(5) Å, comparable to that found in $\text{Cp}(\text{CO})\text{FeH}(\text{SnEt}_3)(\text{GeEt}_3)$ ($d_{\text{Sn-H}} = 2.16$ (13) Å).^{35d} In the related hydrido iron(IV) complexes, the Fe(IV)–H bond lengths are between 1.24 and 1.72 Å.³⁸ The Fe–H bond length of 1.28(5) Å agrees with the assignment of an iron(IV) species, and the involvement of the η^2 -coordination mode of the H–Sn bond can be negligible.

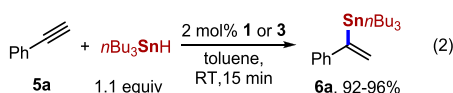
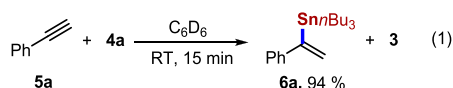
When coordinating the E–H bond to a metal center, forming a σ -complex is usually prior to the bond oxidative addition.³⁹ Although complex **4a** features the structural characteristics of an iron(IV) hydride, at low temperatures it is converted reversibly to the nonclassical σ -stannane complex (**4b**), with which it maintains a tautomeric equilibrium (Scheme 3). Upon cooling a d_8 -toluene solution of **4a** to 233 K, the ^1H NMR spectrum indicates that the solution contains two hydride species. In addition to the signal displayed at δ –12.3 (d, $J_{\text{P-H}} = 68$ Hz) for **4a**, a new hydride signal appeared at δ –11.2 (d, $J_{\text{P-H}} = 53$ Hz) for **4b** (Figure 3), corresponding to the ^{31}P signal at δ 88.2. At 213 K, this new signal is well-resolved as a sharp doublet flanked by a tin

Scheme 3. Interconversions between the Iron(IV) Hydride and the σ -Complex



satellite ($J_{\text{Sn-H}} = 330$ Hz), while the ^{119}Sn resonances were observed at δ 203.4 (d, $J_{\text{P-Sn}} = 624$ Hz, $\text{Sn}n\text{Bu}_2$) and 61.2 (d, $J_{\text{P-Sn}} = 132$ Hz, $\sigma\text{-H-Sn}n\text{Bu}_3$). The pattern of the hydride resonance of **4b** is very similar to that of the σ -stannane complex [$\text{Cp}^*\text{RuCl}(\text{iPr}_3\text{P})(\eta^2\text{-H-Sn}n\text{Bu}_3)$],^{26b} and the $J_{\text{Sn-H}}$ coupling constants lie between 90 and 440 Hz.^{26b,40} Consequently, it was inferred that a η^2 -coordinated hydrostannane existed at the iron center. After the NMR solution was warmed to room temperature, only **4a** was detected, implying the completion of the oxidative addition of the Sn-H bond. The free energy change for the reversible Sn-H bond cleavage at the iron center was estimated to be -0.46 kcal/mol at 233 K based on the equilibrium ratio of **4a/4b** = 1:2.7.

Complex **4a** can hydrostannate alkynes. For instance, the reaction of **4a** with an equimolar amount of phenylacetylene (**5a**) in C_6D_6 completes within several minutes, and ^{31}P NMR spectroscopic studies suggested the full conversion of **4a** to **3**. The organotin product, α -tributyl(1-phenylvinyl)stannane (**6a**), formed in 94% yield, was isolated and identified by ^1H NMR spectroscopy (eq 1). More importantly, both **1** and **3** are



efficient catalysts in the α -hydrostannation of 1-alkynes. Upon loading 2 mol % of **3** with 1.1 equiv of $n\text{Bu}_3\text{SnH}$ in toluene, the reaction of **5a** exclusively produced **6a** in 92% isolated yield (eq 2) within 15 min. Using **1** as a catalyst, the reaction of **5a** under identical conditions also led to fast α -hydrostannation producing the products with 96% yields.

Catalytic Markovnikov Hydrostannation of Alkynes.

Since the sequential conversions of **1** to **4** through **3** by excess $n\text{Bu}_3\text{SnH}$ are fast, we chose **1** as the catalyst precursor to examine the alkyne scope. As shown in Table 1, aromatic alkynes with either electron-withdrawing or electron-donating substituents at various positions in the aromatic ring of phenylacetylene allow for hydrostannation under the catalytic conditions, providing α -vinylstannanes in good yields and with high regio- and chemoselectivity. In addition to halogen groups (**6d**, **6e**, **6k**, **6m**, and **6n**), functional groups including $-\text{NH}_2$ (**6j**), $-\text{COOMe}$ (**6l**), and $-\text{OH}$ groups (**6o**) are tolerated well in the reaction. 4-Ethynyl-*N,N*-dimethylaniline, which was difficult to undergo hydrostannation in the trityl-cation-mediated hydrostannation,⁴¹ is efficiently converted to the α -vinylstannane (**6c**) in 97% yield by this iron-catalyzed protocol. In the reaction of *p*-trifluorophenylacetylene, the α -product **6g** was obtained as a major product with a small amount of inseparable β -product ($\alpha:\beta = 96:4$). Such regioselective hydrostannation was also found in the case of 1-ethynyl-4-nitrobenzene and 4-ethynylbenzaldehyde, which provided the corresponding α -vinylstannanes (**6h** and **6i**, respectively) as major products. Selective hydrometalation of alkynes containing $-\text{CHO}$ and $-\text{NO}_2$ groups are extremely challenging since they are prone to reduction. Both of the entities were retained, however, in this transformation. 1-Alkynes functionalized by naphthyl (**6p**), phenanthryl (**6q**), thienyl (**6r**, **6s**), and ferrocenyl (**6t**) groups underwent

Table 1. Fe-Catalyzed α -Hydrostannation of Alkynes^a

Aryl alkyne variation

6a , 96%	6b , 97%	6c , 97%	6d , 96%
6e , 92%	6f , 84%	6g , 85% (96:4) ^b	6h , 87% (89:11) ^b
6i , 88% (90:10) ^b	6j , 86%	6k , 90%	6l , 91%
6m , 94%	6n , 95%	6o , 81%	6p , 95%
6q , 84%	6r , 80%	6s , 88%	6t , 96%

Alkyl alkyne variation

6u , 90%	6v , 85%	6w , 89%	6x , 85%
6y , 84%	6z , 87%	6aa , 81%	
6ab , 94%	6ac , 96%	6ad , 94%	6ae , 90%

^aReaction conditions: catalyst **1** (4 μmol , 2 mol %) and $n\text{Bu}_3\text{SnH}$ (0.22 mmol) were dissolved in toluene (0.3 mL), and the alkyne substrate (0.2 mmol) in 0.2 mL toluene was added dropwise and stirred for 15 min at room temperature. Isolated yields are given.

^bThe α/β ratios given in parentheses were determined by ^1H NMR spectra of the isolated mixtures.

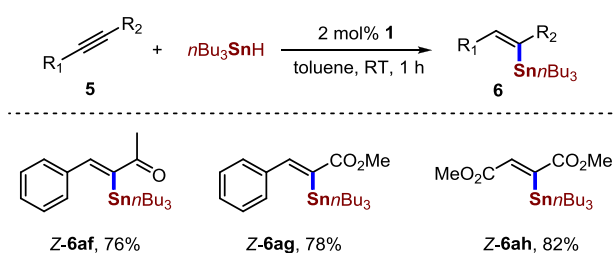
hydrostannation smoothly, giving the α -vinylstannane products in good yields.

Remarkably, the present iron-catalyzed protocol can also be used for the transformation of aliphatic alkynes. The reactions of linear chain alkynes, 1-hexyne and 1-decyne, produced the aliphatic α -vinylstannanes **6u** and **6v** in 90% and 85% yield, respectively. Hydrostannation of 3-phenyl-1-propyne furnished the α -product (**6w**) in 89% yield. Aliphatic alkynes with functional groups such as benzyl ether (**6x**), iodophenol ether (**6y**), and indolyl (**6z**) were generally well tolerated. The hydrostannation was also achieved in the presence of an unprotected alcohol group (**6aa**). The regioselective Sn-H

addition was not impeded by the steric hindrance of the substrate, as exemplified by branched alkynes (**6ab–6ae**). The C≡C triple bond was chemo- and regioselectively hydro-metallated for a conjugated enyne to afford the organotin-functionalized diene (**6ab**) in 94% yield. Importantly, cyclopropylvinylstannane (**6ac**) was obtained in 96% yield in the reaction with cyclopropylacetylene, and no ring-opening product was detected. In the case of [Fe–Cu]-catalyzed hydrostannation, the reaction of 3,3-dimethylbut-1-yne was found to give (*E*)- β -vinylstannane in low yield.³⁰ In contrast, the present iron-based transformation exclusively provides α -vinylstannanes (**6ae**).

Addition of $n\text{Bu}_3\text{SnH}$ to α,β -unsaturated alkynes by using catalyst **1** was also examined. Although the production of vinylstannane was not observed from 1-phenylprop-1-yne and diphenylethyne, the expected iron-catalyzed Sn–H addition proceeded successfully with alkynyl ketones and esters, a generally reliable substrate class (Table 2). In the presence of 2

Table 2. Hydrostannation of α,β -Unsaturated Alkynes^a



^aReaction conditions were identical to those described in Table 1; reaction time was 1 h; and isolated yields are provided.

mol % of **1**, the reaction of 4-phenylbut-3-yn-2-one with $n\text{Bu}_3\text{SnH}$ at room temperature for 1 h afforded the α,β -unsaturated organotin compound **Z-6af** in 76% yield with excellent regioselectivity and a high degree of diastereoselectivity. Similar anti-hydrostannation was also observed for alkynoates represented by **Z-6ag** and **Z-6ah**, providing the (*Z*)- α -stannyl enoate products in moderate yields.

Activation of 1-Alkynes. Activating terminal alkynes by a transition-metal complex potentially provides access to metal alkynyl,⁴² vinylidene,⁴³ or vinyl intermediates,⁴⁴ which are widely involved in alkyne functionalization reactions. We found that both the iron–amido and iron–aryloxo complexes are capable of activating terminal alkynes, affording iron vinyl (**7**) and iron vinylidene (**8**) intermediates, respectively (Scheme 4).

Monitored by ³¹P NMR spectra, the reaction of **1** or **2** in toluene with **5a** led to the clean formation of the corresponding low-spin iron(II) compounds **7** and **8** respectively after 12 h (Figures S34 and S39). The ESI-MS

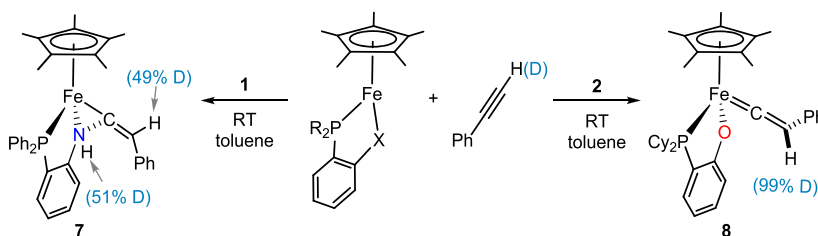
spectral analysis of the reaction solutions features a peak at m/z 570.1996 for **7** and m/z 582.2704 for **8**, indicative of incorporation of the alkyne into the corresponding parent complex (Figures S36 and S41). The aminovinyl and vinylidene moieties in the resulting complexes were inferred from the ¹H and ¹³C NMR spectra. The α -vinyl carbon resonance in **7** was observed as a doublet at δ 196.3 ($J_{\text{P-C}} = 25$ Hz), compared to the doublet at δ 357.3 ($J_{\text{P-C}} = 38$ Hz) for the α -vinylidene carbon in **8**. In the ¹H NMR spectra of **8**, the vinyl proton signal was displayed as a doublet at δ 5.62 (d, $J_{\text{P-H}} = 5.1$ Hz), consistent with the patterns that have been reported for transition-metal vinylidene complexes.⁴⁵ In contrast, the aminovinyl proton signal of **7** at δ 7.31 is obscured by the distinct phenyl proton signals in the ¹H NMR spectrum but was unambiguously observed in the ²H NMR spectrum of **1** with $\text{PhC}\equiv\text{CD}$ (**d-5a**, *vide infra*).

The synergistic Fe–X bond reactivity was further demonstrated by the deuterated 1-alkyne activation. For the reaction of **1** with **d-5a**, deuterium incorporation was observed at the positions of the amino site (δ 3.05, 51% *d*-enriched) and β -vinyl carbon (δ 7.31, 49% *d*-enriched), in almost a 1:1 ratio (Figure S37). In the reaction with **2**, the ²H NMR spectrum exhibits only a characteristic vinyl ²H signal at δ 5.68 (Figure S42). According to the NMR results, it is proposed that activation of the C(sp)–H bond at the Fe–X site results in the formation of the iron–alkynyl intermediate $\text{Cp}^*\text{Fe}(\text{C}\equiv\text{CPh})(1,2\text{-R}_2\text{PC}_6\text{H}_4\text{XH})$, which then rearranges to an iron(II) vinylidene complex. In contrast to the aryloxo in **8**, the amino group of **7** not only serves as a Lewis base to facilitate proton shuttling but also behaves as a nucleophile which attacks the vinylidene α -carbon resulting in an intramolecular N–C bond formation.

The solid-state structures of **7** and **8** were confirmed by crystallographic analysis (Figure 4). In **7**, the N atom is attached to the α -vinyl carbon ($d_{\text{N-C29}} = 1.477(2)$ Å), forming a genuine three-membered Fe–N–C metallic-heterocycle, but the phenyl vinylidene ligand in **8** is solely coordinated to the Fe center as an unsaturated carbene with $\angle\text{Fe-C29-C30} = 170.3(4)^\circ$. The Fe–C29 distances in the two complexes differ significantly and are 1.851(2) Å for **7** vs 1.737(4) Å for **8**. For complex **8**, especially, the Fe–C29 bond length is in the range of 1.68–1.77 Å reported for the vinylidene complexes,⁴⁵ and the C29–C30 bond length of 1.321(6) Å suggests a double bond character.

As a consequence of the striking structural differences, the reactive nature of the two organoiron species (**7** and **8**) toward $n\text{Bu}_3\text{SnH}$ differs greatly. The iron vinyl complex (**7**) was found to be stable toward the tin hydride, and no reaction was observed (eq 3). In contrast, the stoichiometric reaction between the vinylidene compound (**8**) and $n\text{Bu}_3\text{SnH}$ produced (*E*)-tributyl(styryl)stannane (**E-9a**, >98%) which was identi-

Scheme 4. Activation of Phenylacetylene by **1 and **2****



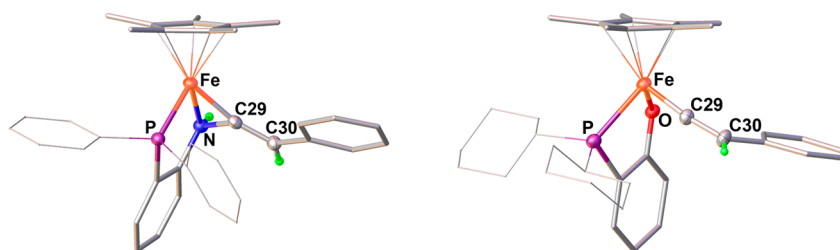
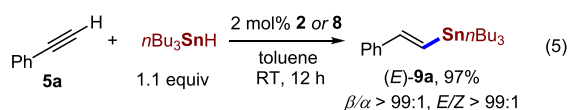
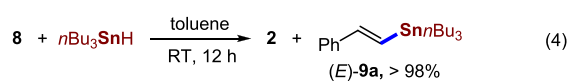
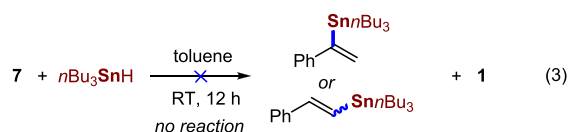


Figure 4. Solid-state structures of **7** (left) and **8** (right). Selected bond distances (Å) and angles (deg): for **7**, Fe–P 2.1620(5), Fe–N 2.015(1), Fe–C29 1.851(2), N–C29 1.477(2), C29–C30 1.335(3), P–Fe–N 84.41(5), C29–Fe–N 44.66(7), Fe–C29–C30 162.7(1); for **8**, Fe–P 2.240(1), Fe–O 1.973(3), Fe–C29 1.737(4), C29–C30 1.321(6), P–Fe–O 81.97(9), Fe–C29–C30, 170.3(4).



fied by its ^1H NMR spectrum (eq 4). The ESI-MS spectrum showed a peak at m/z 480.2206 that indicates complex **2**. Further treatment of the reaction solution with **5a** led to the recovery of **8**. The generation of **2** was also trapped by 1-ethynylferrocene to form a new iron vinylidene complex (**10**), which was also structurally characterized by single-crystal X-ray crystallographic analysis (Figure S4).

Anti-Markovnikov Hydrostannation of Alkynes. Based on the activation of 1-alkynes and the fundamental conversions between the iron aryloxide complexes **8** and **2**, we achieved the catalytic anti-Markovnikov hydrostannation of 1-alkynes (eq 5). Using 2 mol % of **2** (or **8**) as catalyst, the reaction of **5a** (0.2 mmol) with $n\text{Bu}_3\text{SnH}$ (0.22 mmol) for 12 h provided *E*-**9a** in high yield and with excellent regio- and stereoselectivity (97% yield, $\beta/\alpha > 99:1$, *E/Z* > 99:1). Several 1-alkynes bearing different functional groups were subjected to the reaction catalyzed by **2** (Table 3).

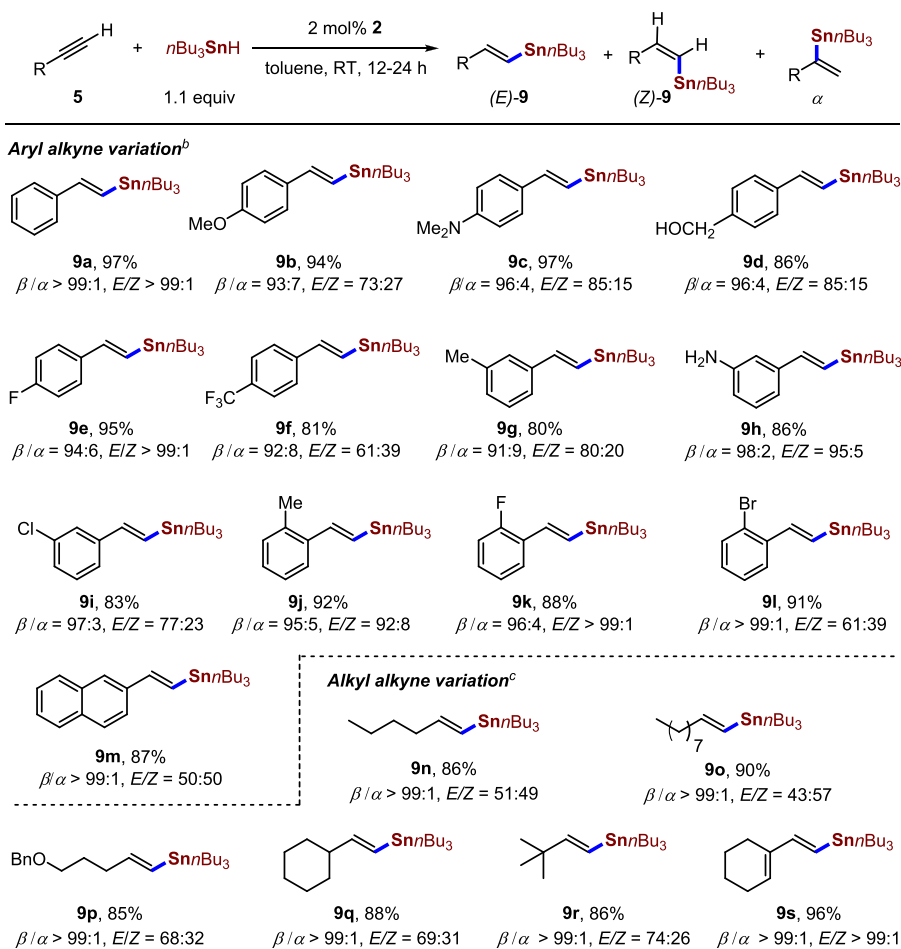
Generally, most of the aryl-substituted 1-alkynes examined in the iron(II)–amido catalysis react smoothly with $n\text{Bu}_3\text{SnH}$ by this iron–aryloxide protocol to afford (*E*)- β -vinylstannanes (**9a**–**9m**) as the major product. Modifying the substitution on the aromatic ring with a variety of electron-donating and electron-withdrawing groups, such as OMe (**9b**), Me (**9g** and **9j**), NMe₂ (**9c**), F (**9e** and **9k**), Cl (**9i**), Br (**9l**), and CF₃ (**9f**), does not affect the outcome of the reaction much. Notably, unprotected hydroxyl (**9d**) and amino (**9h**) groups were tolerated in the β -hydrostannation. The reaction of 2-ethynyl-naphthalene provided β -vinylstannanes composed of two stereoisomers with *E/Z* in almost a 1:1 ratio. This iron–aryloxide protocol was also applicable to aliphatic 1-alkynes with high regioselectivity. Hydrostannation of linear chain alkynes such as 1-hexyne, 1-decyne, and a benzyl ether substituted 1-pentyne furnished the β -vinylstannanes **9n**, **9o**, and **9p** in 86%, 90%, and 85% yield, respectively. Steric hindrance has no effect on regioselectivity but affects the

stereoselectivity and is exemplified by reactions of secondary and tertiary alkyl alkynes to produce the (*E*)-isomers as the major products (**9q**, **9r**). Conjugated enynes are compatible with the hydrostannation conditions and afford the desired vinyl-functionalized diene (**9s**) in 96% yield and excellent regio- and stereoselectivity. Internal alkynes did not react with tin hydride under these conditions, consistent with the observations that the catalysis proceeds via the iron vinylidene intermediate.

To demonstrate the synthetic utility of the iron-catalyzed protocol, a 1-alkyne substrate derived from estrone (**11**) was subjected to the two reaction conditions by iron–amido and iron–aryloxide catalysis. Divergent vinylstannanes **12a** (495 mg, 87% yield) and **12b** (461 mg, 81% yield) were conveniently synthesized from the scaled-up reactions without significant loss in yield (Scheme 5). Although terminal vinylmetal analogues of **11** have been reported by functionalizing complex organic precursors,⁴⁶ the present transformation provides a general method of synthesizing both α - and β -vinylstannanes.

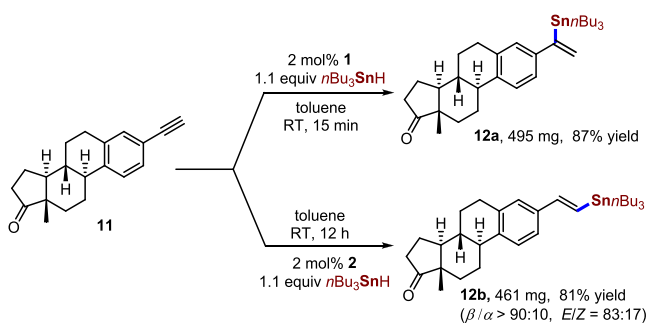
Mechanism. To get more insight into the regio-divergent hydrostannation, deuterium labeling in the hydrostannation of **5a** was investigated (Scheme 6a). Using the deuterated hydrostannane reagent $n\text{Bu}_3\text{SnD}$, the reaction of **5a** catalyzed by **1** led to *d*-**6a** with deuterium incorporation at a *cis*-position relative to the $\text{Sn}n\text{Bu}_3$ moiety. In comparison with **5a**, the reaction of the deuterated alkyne *d*-**5a** with $n\text{Bu}_3\text{SnH}$ afforded α -vinylstannane (*d*-**6a'**) with deuterium at the *trans*-position. These results suggest the iron–amido-catalyzed α -hydrostannation proceeds through the *syn*-addition of the tin hydride across the $\text{C}\equiv\text{C}$ bond (Figure S5). By contrast, in the hydrostannation of **5a** with $n\text{Bu}_3\text{SnD}$ catalyzed by complex **2**, the $n\text{Bu}_3\text{Sn}$ moiety and D atom were both added to the β -carbon to give the gem-product *d*-(*E*)-**9a**. This gem-addition was further confirmed by the reaction of *d*-**5a** with $n\text{Bu}_3\text{SnH}$ to form *d*-(*E*)-**9a'**, in which the hydrogen atom at the α -position is labeled (Figures S6 and S7).

Intermolecular kinetic isotope effects (KIE) experiments were also performed using $n\text{Bu}_3\text{SnH}$ vs $n\text{Bu}_3\text{SnD}$ to reduce **5a** and $n\text{Bu}_3\text{SnH}$ for the hydrostannation of **5a** vs *d*-**5a** (Figures S8–S11). In the iron–amido catalysis, reducing **5a** with an equimolar amount of $n\text{Bu}_3\text{SnH}$ and $n\text{Bu}_3\text{SnD}$ produces **6a** and *d*-**6a** in a 2:1 ratio, giving a KIE value of 2.0. There is no isotopic H/D competition between **5a** and *d*-**5a** in the reaction with $n\text{Bu}_3\text{SnH}$ since **6a** and *d*-**6a'** were produced in almost a 1:1 ratio. In the iron–aryloxide catalysis, by contrast, the intermolecular competitions for the **5a**/*d*-**5a** pair ($k_{\text{H}}/k_{\text{D}} = 2.4$) and $n\text{Bu}_3\text{SnH}/n\text{Bu}_3\text{SnD}$ pair ($k_{\text{H}}/k_{\text{D}} = 2.1$) show mechanistically significant kinetic isotope effects. These results suggest that the cleavage of Sn–H is involved in the turnover-

Table 3. Fe-Catalyzed β -Hydrostannation of Alkynes^a

^aReaction conditions: catalyst **2** (4 μ mol, 2 mol %), alkynes (0.2 mmol), and $n\text{Bu}_3\text{SnH}$ (0.22 mmol) were dissolved in toluene (0.5 mL) and stirred at room temperature. Isolated yields are provided. The β/α and E/Z isomers ratios were determined by ^1H NMR spectra of the isolated mixtures. ^b12 h for aryl-substituted alkynes. ^c24 h for alkyl-substituted alkynes.

Scheme 5. Controlled Regioselective Hydrostannation of the Estrone Derivative



determining step of the α -hydrostannation, while the activation of the $\text{C}(\text{sp})\text{-H}$ bond of the alkyne and the Sn-H addition are both involved in the turnover-limiting formation of the β -vinylstannane.

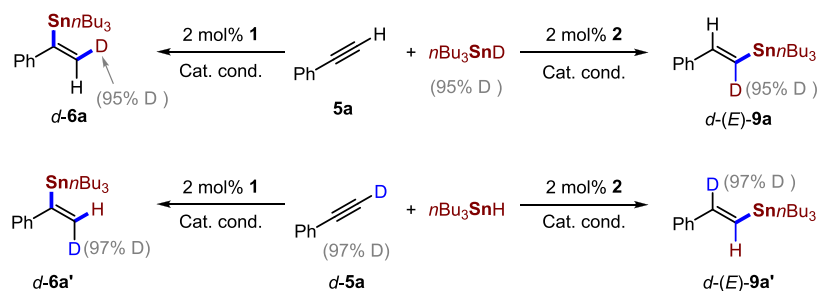
From a mechanistic viewpoint, α -hydrostannation of 1-alkynes processed by the iron-amido complex is initiated by activation of the tin hydride while the β -hydrostannation begins with the substrate activation (Scheme 6b). Although the activation of $n\text{Bu}_3\text{SnH}$ by **1** appears to compete with 1-alkyne, the results of the stoichiometric reactions indicate that the

activation of $n\text{Bu}_3\text{SnH}$ is much faster than that of the 1-alkyne. The activation of the first $n\text{Bu}_3\text{SnH}$ is probably through an intermediate of the iron-stannane adduct [1-HSnBu_3] in which the Sn-H bond is captured at the Fe-N unit (Supporting Information). Due to the strong nucleophilic and anionic nature, the amido site can tightly bind the Sn center, increasing the electron density of stannane and significantly changing its chemical property. Such an iron-stannane adduct seems to favor eliminating butane, leading to the stannyl-iron compound (**3**). By oxidative addition of the second stannane to the iron-stannyl species, distannyl $\text{Fe}(\text{IV})\text{-H}$ (**4a**) is formed as a key intermediate for the hydrometalation reaction. Such iron-based hydrostannation is proposed through a pathway of alkyne insertion into the Fe-SnBu_3 bond to process the stannyl moiety at the internal carbon, producing an β -stannylvinyl iron hydride (**Int 1**).^{24,29} Reductive elimination of the vinylstannane product from **Int 1** results in regeneration of **3** and completes the cycle. Given that highly selective syn-addition products are observed from deuterium-labeling experiments, the outer sphere concerted mechanism delivering the hydride and the $n\text{Bu}_3\text{Sn}$ moiety from distannyl $\text{Fe}(\text{IV})\text{-H}$ to the $\text{C}\equiv\text{C}$ bond cannot be ruled out.

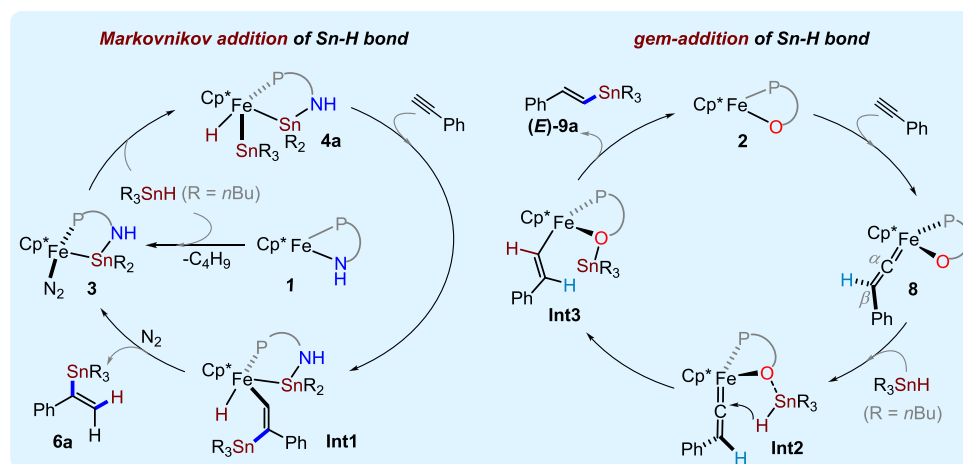
In the β -hydrostannation of 1-alkynes, the formation of the iron vinylidene intermediate (**8**) is essential to the gem-addition.⁴⁷ It is well-known that the α -carbon atom of the

Scheme 6. Mechanistic Insights into Regiodivergent Hydrostannation

a) Deuterium labeling experiments



b) Proposed mechanism for the iron-catalyzed regiodivergent hydrostannation



vinylidene ligand is extremely reactive toward nucleophiles.⁴³ The vinylidene ligand in **8** allows nucleophilic attack at the α -carbon by the tin hydride. We propose that the oxide site facilitates the Sn–H bond cleavage for the hydride transfer through O \rightarrow Sn interaction (**Int 2**) and could capture the stannyl fragment to form the iron vinyl intermediate (**Int 3**). The subsequent transfer of the stannyl fragment to the vinyl moiety produces the β -vinylstannanes and regenerates **2**. The steric factors in **Int 2** more likely control the outcome's stereoselectivity because this, in principle, causes the formation of the two *E* and *Z* stereoisomers. According to the crystal structure of **8**, the Ph group of the vinylidene is close to the O donor. Upon coordination of $n\text{Bu}_3\text{SnH}$, the vinylidene ligand undergoes isomerization to reduce steric repulsion between the Ph group and O– $\text{Sn}n\text{Bu}_3$ moiety.

CONCLUSION

In summary, we report a new type of Cp*Fe(1,2-R₂PC₆H₄X) cooperative catalyst for regiodivergent hydrostannation of alkynes by tuning the Fe–X reactivity. We have demonstrated that the initial step of the catalysis is conveniently controlled by activation of either the tin hydride or the 1-alkyne. The α -hydrostannation originates from the fast Sn–H activation by the iron–amido catalyst to afford the distannyln Fe(IV)–H intermediate. In contrast, the β -hydrostannation proceeding by the iron–aryloxide catalyst arises from transforming RC \equiv CH into the Fe–vinylidene intermediate. The critical feature that distinguishes the iron–amido complex from the iron–aryloxide is that the amido nitrogen can strongly bind the first Sn center, resulting in reductive elimination of butane to

form a new stannyliron species, which, in turn, enables the oxidative addition of the second stannane. Although the iron–aryloxide is inactive for the Sn–H bond cleavage, it can gently activate 1-alkyne through metal–ligand cooperation.

To achieve such iron-based cooperative catalysis, the chemistry at an Fe–X site and the reactivity of the resultant organoiron species are of obvious significance. Although stoichiometric transformations of alkynes to vinylidene complexes have been known for several decades,⁴³ activations of 1-alkynes by iron complexes to afford vinylidene species for catalysis have been only slightly reported.³² The present catalytically regenerated iron vinylidene intermediate might support exploring other important transformations involving alkyne functionalization, and these could expand the scope of iron catalysis in organic synthesis.

ASSOCIATED CONTENT

Supporting Information

The Supporting Information is available free of charge at <https://pubs.acs.org/doi/10.1021/jacs.0c11448>.

Experimental details, characterization, crystallographic data, and ¹H, ¹³C, ³¹P, ¹⁹F, and ¹¹⁹Sn NMR spectra (PDF)

Crystallographic CIF data (CIF)

AUTHOR INFORMATION

Corresponding Authors

Wenguang Wang – School of Chemistry and Chemical Engineering, Shandong University, Jinan 250100, China;

College of Chemistry, Beijing Normal University, Beijing 100875, China; orcid.org/0000-0002-4108-7865;
Email: wwg@sdu.edu.cn

Qing-Xiao Tong – Department of Chemistry, Shantou University, Shantou 515063, China; orcid.org/0000-0002-8125-9684; Email: qxtong@stu.edu.cn

Authors

Jianguo Liu – School of Chemistry and Chemical Engineering, Shandong University, Jinan 250100, China

Heng Song – School of Chemistry and Chemical Engineering, Shandong University, Jinan 250100, China

Tianlin Wang – School of Chemistry and Chemical Engineering, Shandong University, Jinan 250100, China

Jiong Jia – School of Chemistry and Chemical Engineering, Shandong University, Jinan 250100, China

Chen-Ho Tung – School of Chemistry and Chemical Engineering, Shandong University, Jinan 250100, China;
orcid.org/0000-0001-9999-9755

Complete contact information is available at:
<https://pubs.acs.org/10.1021/jacs.0c11448>

Notes

The authors declare no competing financial interest.

ACKNOWLEDGMENTS

We are thankful for the financial support from NSFC (22022102, 22071010, and 21871166), Natural Science Foundation of Shandong Province (ZR2019ZD45), and Pearl River Scholar Funded Scheme 2019 (GDUPS2019).

REFERENCES

- (1) (a) Fulton, J. R.; Sklenak, S.; Bouwkamp, M. W.; Bergman, R. G. A Comprehensive Investigation of the Chemistry and Basicity of a Parent Amidoruthenium Complex. *J. Am. Chem. Soc.* **2002**, *124*, 4722–4737. (b) Fulton, J. R.; Holland, A. W.; Fox, D. J.; Bergman, R. G. Formation, Reactivity, and Properties of Late Transition Metal–Oxygen and -Nitrogen Bonds. *Acc. Chem. Res.* **2002**, *35*, 44–56.
- (2) (a) Hong, S. Y.; Park, Y.; Hwang, Y.; Kim, Y. B.; Baik, M.; Chang, S. Selective Formation of γ -lactams via C–H Amidation Enabled by Tailored Iridium Catalysts. *Science* **2018**, *359*, 1016–1021. (b) Lee, M.; Jung, H.; Kim, D.; Park, J.; Chang, S. Modular Tuning of Electrophilic Reactivity of Iridium Nitrenoids for the Intermolecular Selective α -Amidation of β -Keto Esters. *J. Am. Chem. Soc.* **2020**, *142*, 11999–12004. (c) Lee, J.; Lee, J.; Jung, H.; Kim, D.; Park, J.; Chang, S. Versatile Cp*Co(III)(LX) Catalyst System for Selective Intramolecular C–H Amidation Reactions. *J. Am. Chem. Soc.* **2020**, *142*, 12324–12332.
- (3) (a) Chalkley, M. J.; Drover, M. W.; Peters, J. C. Catalytic N₂-to-NH₃ (or -N₂H₄) Conversion by Well-Defined Molecular Coordination Complexes. *Chem. Rev.* **2020**, *120*, 5582–5636. (b) Nesbit, M. A.; Oyala, P. H.; Peters, J. C. Characterization of the Earliest Intermediate of Fe–N₂ Protonation: CW and Pulse EPR Detection of an Fe–NNH Species and Its Evolution to Fe–NNH₂⁺. *J. Am. Chem. Soc.* **2019**, *141*, 8116–8127. (c) Thompson, N. B.; Green, M. T.; Peters, J. C. Nitrogen Fixation via a Terminal Fe(IV) Nitride. *J. Am. Chem. Soc.* **2017**, *139*, 15312–15315.
- (4) Zuo, W.; Lough, A. J.; Li, Y. F.; Morris, R. H. Amine(imine)-diphosphine Iron Catalysts for Asymmetric Transfer Hydrogenation of Ketones and Imines. *Science* **2013**, *342*, 1080–1083.
- (5) (a) Drover, M. W.; Love, J. A.; Schafer, L. L. Toward Anti-Markovnikov 1-Alkyne O-Phosphoramidation: Exploiting Metal-Ligand Cooperativity in a 1,3-N,O-Chelated Cp*Ir(III) Complex. *J. Am. Chem. Soc.* **2016**, *138*, 8396–8399. (b) Drover, M. W.; Love, J. A.; Schafer, L. L. 1,3-N,O-Complexes of Late Transition Metals.

Ligands with Flexible Bonding Modes and Reaction Profiles. *Chem. Soc. Rev.* **2017**, *46*, 2913–2940.

(6) Zhao, B.; Han, Z.; Ding, K. The N–H Functional Group in Organometallic Catalysis. *Angew. Chem., Int. Ed.* **2013**, *52*, 4744–4788.

(7) Chakraborty, S.; Brennessel, W. W.; Jones, W. D. A Molecular Iron Catalyst for the Acceptorless Dehydrogenation and Hydrogenation of N-Heterocycles. *J. Am. Chem. Soc.* **2014**, *136*, 8564–8567.

(8) Chakraborty, S.; Dai, H.; Bhattacharya, P.; Fairweather, N. T.; Gibson, M. S.; Krause, J. A.; Guan, H. Iron-Based Catalysts for the Hydrogenation of Esters to Alcohols. *J. Am. Chem. Soc.* **2014**, *136*, 7869–7872.

(9) Kovacs, J. A.; Brines, L. M. Understanding How the Thiolate Sulfur Contributes to the Function of the Non-Heme Iron Enzyme Superoxide Reductase. *Acc. Chem. Res.* **2007**, *40*, 501–509.

(10) Omann, L.; Königs, C. D. F.; Klare, H. F. T.; Oestreich, M. Cooperative Catalysis at Metal–Sulfur Bonds. *Acc. Chem. Res.* **2017**, *50*, 1258–1269.

(11) (a) Zhang, F.; Song, H.; Zhuang, X.; Tung, C.-H.; Wang, W. Iron-Catalyzed 1,2-Selective Hydroboration of N-Heteroarenes. *J. Am. Chem. Soc.* **2017**, *139*, 17775–17778. (b) Song, H.; Ye, K.; Geng, P.; Han, X.; Liao, R.; Tung, C.-H.; Wang, W. Activation of Epoxides by a Cooperative Iron–Thiolate Catalyst: Intermediacy of Ferrous Alkoxides in Catalytic Hydroboration. *ACS Catal.* **2017**, *7*, 7709–7717. (c) Hou, S.; Chen, J. Y.; Xue, M.; Jia, M.; Zhai, X.; Liao, R. Z.; Tung, C.-H.; Wang, W. Cooperative Molybdenum–Thiolate Reactivity for Transfer Hydrogenation of Nitriles. *ACS Catal.* **2020**, *10*, 380–390.

(12) Chu, W. Y.; Zhou, X.; Rauchfuss, T. B. Cooperative Metal–Ligand Reactivity and Catalysis in Low-Spin Ferrous Alkoxides. *Organometallics* **2015**, *34*, 1619–1626.

(13) (a) Blacquiere, J. M.; McDonald, R.; Fogg, D. E. Integrating the Schrock and Grubbs Catalysts: Ruthenium–Binaphtholate Catalysts for Olefin Metathesis. *Angew. Chem., Int. Ed.* **2010**, *49*, 3807–3810. (b) Blacquiere, J. M.; Higman, C. S.; McDonald, R.; Fogg, D. E. A Reactive Ru–Binaphtholate Building Block with Self-Tuning Hapticity. *J. Am. Chem. Soc.* **2011**, *133*, 14054–14062.

(14) Liu, J.; Chen, J. Y.; Jia, M.; Ming, B.; Jia, J.; Liao, R. Z.; Tung, C.-H.; Wang, W. Ni–O Cooperation versus Nickel(II) Hydride in Catalytic Hydroboration of N-Heteroarenes. *ACS Catal.* **2019**, *9*, 3849–3857.

(15) Tard, C.; Pickett, C. J. Structural and Functional Analogues of the Active Sites of the [Fe]-, [NiFe]-, and [FeFe]-Hydrogenases. *Chem. Rev.* **2009**, *109*, 2245–2274.

(16) Hoffman, B. M.; Lukoyanov, D.; Yang, Z. Y.; Dean, D. R.; Seefeldt, L. C. Mechanism of Nitrogen Fixation by Nitrogenase: The Next Stage. *Chem. Rev.* **2014**, *114*, 4041–4062.

(17) (a) Gloaguen, F.; Rauchfuss, T. B. Small Molecule Mimics of Hydrogenase: Hydrides and Redox. *Chem. Soc. Rev.* **2009**, *38*, 100–108. (b) Schilter, D.; Camara, J. M.; Huynh, M. T.; Hammes-Schiffer, S.; Rauchfuss, T. B. Hydrogenase Enzymes and Their Synthetic Models: The Role of Metal Hydrides. *Chem. Rev.* **2016**, *116*, 8693–874.

(18) Selected examples for iron-based metal–ligand strategy: (a) Morris, R. H. Exploiting Metal–Ligand Bifunctional Reactions in the Design of Iron Asymmetric Hydrogenation Catalysts. *Acc. Chem. Res.* **2015**, *48*, 1494–1502. (b) Zell, T.; Milstein, D. Hydrogenation and Dehydrogenation Iron Pincer Catalysts Capable of Metal–Ligand Cooperation by Aromatization/Dearomatization. *Acc. Chem. Res.* **2015**, *48*, 1979–1994. (c) Pellissier, H. Recent Developments in Enantioselective Iron-catalyzed Transformations. *Coord. Chem. Rev.* **2019**, *386*, 1–31.

(19) Wei, D.; Darcel, C. Iron Catalysis in Reduction and Hydrometallation Reactions. *Chem. Rev.* **2019**, *119*, 2550–2610.

(20) Stille, J. K. The Palladium-Catalyzed Cross-Coupling Reactions of Organotin Reagents with Organic Electrophiles. *Angew. Chem., Int. Ed. Engl.* **1986**, *25*, 508–524.

(21) (a) Matsubara, S.; Hibino, J.; Morizawa, Y.; Oshima, K.; Nozaki, H. Regio- and Stereo-selective Synthesis of Vinylstannanes.

Transition-metal Catalyzed Stannylation of Acetylenes and Conversion of Enol Triflates and Vinyl Iodides into Vinylstannanes. *J. Organomet. Chem.* **1985**, *285*, 163–172. (b) Sharma, S.; Oehlschlager, A. C. Control of Regiochemistry in Bismetallation of 1-Decyne. *Tetrahedron Lett.* **1986**, *27*, 6161–6164. (c) Sharma, S.; Oehlschlager, A. C. Regioselective Synthesis and Cross Coupling Reactions of 1,2-Borostannyl-1-alkenes. *Tetrahedron Lett.* **1988**, *29*, 261–264. (d) Sharma, S.; Oehlschlager, A. C. Scope and Mechanism of Stannylation of 1-Alkynes. *J. Org. Chem.* **1989**, *54*, 5064–5073. (e) Yoshida, H.; Shinke, A.; Kawano, Y.; Takaki, K. Copper-Catalyzed α -Selective Hydrostannylation of Alkynes for the Synthesis of Branched Alkenylstannanes. *Chem. Commun.* **2015**, *51*, 10616–10619.

(22) (a) Trost, B. M.; Ball, Z. T. Addition of Metalloid Hydrides to Alkynes: Hydrometallation with Boron, Silicon, and Tin. *Synthesis* **2005**, *2005*, 853–887. (b) Smith, N. D.; Mancuso, J.; Lautens, M. Metal-Catalyzed Hydrostannations. *Chem. Rev.* **2000**, *100*, 3257–3282. (c) Alami, M.; Hamze, A.; Provot, O. Hydrostannylation of Alkynes. *ACS Catal.* **2019**, *9*, 3437–3466.

(23) Shibata, I.; Suwa, T.; Ryu, K.; Baba, A. Selective α -Stannylation Addition of Di-*n*-butyliodotin Hydride Ate Complex to Simple Aliphatic Alkynes. *J. Am. Chem. Soc.* **2001**, *123*, 4101–4102.

(24) (a) Zhang, H. X.; Guibé, F.; Balavoine, G. Palladium Catalyzed Hydrostannylation of Alkynes and Palladium-Catalyzed Hydrostannylation of Propargyl or Propargyloxycarbonyl Derivatives of Various Functional Groups. *Tetrahedron Lett.* **1988**, *29*, 619–622. (b) Alami, M.; Liron, F.; Gervais, M.; Peyrat, J.; Brion, J. *Ortho* Substituents Direct Regioselective Addition of Tributyltin Hydride to Unsymmetrical Diaryl (or Heteroaryl) Alkynes: An Efficient Route to Stannylated Stilbene Derivatives. *Angew. Chem., Int. Ed.* **2002**, *41*, 1578–1580. (c) Debrauwer, V.; Turlik, A.; Rummel, L.; Prescimone, A.; Blanchard, N.; Houk, N. K.; Bizet, V. Ligand-Controlled Regiodivergent Palladium-Catalyzed Hydrogermylation of Ynamides. *J. Am. Chem. Soc.* **2020**, *142*, 11153–11164.

(25) (a) Wesquet, A. O.; Kazmaier, U. Improved Protocols for Molybdenum- and Tungsten-Catalyzed Hydrostannations. *Adv. Synth. Catal.* **2009**, *351*, 1395–1404. (b) Maity, P.; Klos, M. R.; Kazmaier, U. Syntheses of α -Stannylated and α -Iodinated Enamides via Molybdenum-Catalyzed Hydrostannylation. *Org. Lett.* **2013**, *15*, 6246–6249. (c) Mandla, K. A.; Moore, C. E.; Rheingold, A. L.; Figueroa, J. S. Regioselective Formation of (*E*)- β -Vinylstannanes with a Topologically Controlled Molybdenum-Based Alkyne Hydrostannylation Catalyst. *Angew. Chem., Int. Ed.* **2018**, *57*, 6853–6857.

(26) (a) Rummelt, S. M.; Fürstner, A. Ruthenium-Catalyzed *trans*-Selective Hydrostannylation of Alkynes. *Angew. Chem., Int. Ed.* **2014**, *53*, 3626–3630. (b) Rummelt, S. M.; Radkowski, K.; Roşca, D. A.; Fürstner, A. Interligand Interactions Dictate the Regioselectivity of *trans*-Hydrometalations and Related Reactions Catalyzed by [Cp**Ru*Cl]. Hydrogen Bonding to a Chloride Ligand as a Steering Principle in Catalysis. *J. Am. Chem. Soc.* **2015**, *137*, 5506–5519. (c) Roşca, D. A.; Radkowski, K.; Wolf, L. M.; Wagh, M.; Goddard, R.; Thiel, W.; Fürstner, A. Ruthenium-Catalyzed Alkyne *trans*-Hydrometallation: Mechanistic Insights and Preparative Implications. *J. Am. Chem. Soc.* **2017**, *139*, 2443–2455. (d) Fürstner, A. *trans*-Hydrogenation, *gem*-Hydrogenation, and *trans*-Hydrometallation of Alkynes: An Interim Report on an Unorthodox Reactivity Paradigm. *J. Am. Chem. Soc.* **2019**, *141*, 11–24.

(27) Leung, L. T.; Leung, S. K.; Chiu, P. Copper-Catalyzed Hydrostannylation of Activated Alkynes. *Org. Lett.* **2005**, *7*, 5249–5252.

(28) Magre, M.; Szewczyk, M.; Rueping, M. Magnesium-Catalyzed Stereoselective Hydrostannylation of Internal and Terminal Alkynes. *Org. Lett.* **2020**, *22*, 1594–1598.

(29) (a) Trebbe, R.; Schager, F.; Goddard, R.; Pörschke, K. *cis*-($R^2_2PC_2H_4PR^2$)PdH(SnR₃) Complexes: Trapped Intermediates in the Palladium-Catalyzed Hydrostannylation of Alkynes. *Organometallics* **2000**, *19*, 521–526. (b) Hayashi, K.; Iyoda, J.; Shiihara, I. Reaction of Organotin Oxides, Alkoxides and Acyloxides with Organosilicon Hydrides. New Preparative Method of Organotin Hydrides. *J. Organomet. Chem.* **1967**, *10*, 81–94. (c) Ichinose, Y.; Oda, H.;

Oshima, K.; Utimoto, K. Palladium Catalyzed Hydrostannylation and Hydrogermylation of Acetylenes. *Bull. Chem. Soc. Jpn.* **1987**, *60*, 3468–3470.

(30) Cheng, L.-J.; Mankad, N. P. Heterobimetallic Control of Regioselectivity in Alkyne Hydrostannylation: Divergent Syntheses of α - and (*E*)- β -Vinylstannanes via Cooperative Sn–H Bond Activation. *J. Am. Chem. Soc.* **2019**, *141*, 3710–3716.

(31) Forster, F.; López, V. M. R.; Oestreich, M. Catalytic Dehydrogenative Stannylation of C(sp)³–H Bonds Involving Cooperative Sn–H Bond Activation of Hydrostannanes. *J. Am. Chem. Soc.* **2018**, *140*, 1259–1262.

(32) (a) Rivada-Wheelaghan, O.; Chakraborty, S.; Shimon, L. J. W.; Ben-David, Y.; Milstein, D. Z-Selective (Cross-)Dimerization of Terminal Alkynes Catalyzed by an Iron Complex. *Angew. Chem., Int. Ed.* **2016**, *55*, 6942–6945. (b) Gorgas, N.; Alves, L. G.; Stöger, B.; Martins, A. M.; Veiros, L. F.; Kirchner, K. Stable, Yet Highly Reactive Nonclassical Iron(II) Polyhydride Pincer Complexes: Z-Selective Dimerization and Hydroboration of Terminal Alkynes. *J. Am. Chem. Soc.* **2017**, *139*, 8130–8133. (c) Gorgas, N.; Stöger, B.; Veiros, L. F.; Kirchner, K. Iron(II) Bis(acetylide) Complexes as Key Intermediates in the Catalytic Hydrofunctionalization of Terminal Alkynes. *ACS Catal.* **2018**, *8*, 7973–7982. (d) Bridge, B. J.; Boyle, P. D.; Blacquiére, J. M. endo-Selective Iron Catalysts for Intramolecular Alkyne Hydrofunctionalization. *Organometallics* **2020**, *39*, 2570–2574.

(33) (a) Liang, Q.; Sheng, K.; Salmon, A.; Zhou, V. Y.; Song, D. Active Iron(II) Catalysts toward *gem*-Specific Dimerization of Terminal Alkynes. *ACS Catal.* **2019**, *9*, 810–818. (b) Liang, Q.; Hayashi, K.; Rabeda, K.; Jimenez-Santiago, J. L.; Song, D. Piano-Stool Iron Complexes as Precatalysts for *gem*-Specific Dimerization of Terminal Alkynes. *Organometallics* **2020**, *39*, 2320–2326. (c) Ohki, Y.; Hatanaka, T.; Tatsumi, K. C–H Bond Activation of Heteroarenes Mediated by a Half-Sandwich Iron Complex of N-Heterocyclic Carbene. *J. Am. Chem. Soc.* **2008**, *130*, 17174–17186.

(34) (a) Holt, M. S.; Wilson, W. L.; Nelson, J. H. Transition Metal Chemistry. *Chem. Rev.* **1989**, *89*, 11–49. (b) Gorsich, R. D. Preparation and Properties of Some Mixed Metal Carbonyl Compounds. I. Compounds Containing a Group IV Metal and Manganese or Iron. *J. Am. Chem. Soc.* **1962**, *84*, 2486–2491.

(35) (a) Gordon, C.; Schubert, U. Transition-metal Silyl Complexes 51. Preparation of the Mixed Silyl/Stannylation Complexes (π -C₃H₅)Fe(CO)(SnPh₃)(SiR₃)H. *Inorg. Chim. Acta* **1994**, *224*, 177–179. (b) Akita, M.; Oku, T.; Moro-oka, Y. Oxymethylation of Iron Complexes [(Cp)Fe(CO)₂(R)] with HMMe₃ (M = Sn, Si; Cp = C₃H₅) Leading to R-CH₂OH via a Formylation-hydrometallation Sequence. *J. Chem. Soc., Chem. Commun.* **1989**, 1790–1792. (c) Zhang, S.; Brown, T. L. Photochemical Reactions of Cp₂Fe₂(CO)₄ with HSnBu₃. *Organometallics* **1992**, *11*, 2122–2128. (d) Itazaki, M.; Kamitani, M.; Ueda, K.; Nakazawa, H. Syntheses and Ligand Exchange Reaction of Iron(IV) Complexes with Two Different Group 14 Element Ligands, Cp(CO)FeH(EEt₃)(E'Et₃) (E, E' = Si, Ge, Sn). *Organometallics* **2009**, *28*, 3601–3603. (e) Vyboishchikov, S. F.; Nikonov, G. I. Unique {H(SiR₃)₂}, (H₂SiR₃), H(HSiR₃), and (H₂)SiR₃ Ligand Sets Supported by the {Fe(Cp)(L)} Platform (L = CO, PR₃). *Chem. - Eur. J.* **2006**, *12*, 8518–8533.

(36) (a) Sharma, H. K.; Arias-Ugarte, R.; Metta-Magana, A. J.; Pannell, K. H. Dehydrogenative Dimerization of Di-*tert*-butyltin Dihalide Photochemically and Thermally Catalyzed by Iron and Molybdenum Complexes. *Angew. Chem., Int. Ed.* **2009**, *48*, 6309–6312. (b) Sharma, H. K.; Pannell, K. H. The Photochemical Irradiation of R₃SiH in the Presence of [(η^5 -C₃H₅)Fe(CO)₂CH₃] in DMF Leads to Disiloxanes not Disilanes. *Angew. Chem., Int. Ed.* **2009**, *48*, 7052–7054.

(37) Akita, M.; Oku, T.; Tanaka, M.; Morooka, Y. Oxymethylation of Alkyliron Complex CpFe(CO)₂-R with Hydrostannane and -Silane, Leading to R-CH₂OH Derivatives: Related Reactions of CpFe(CO)(L)-R and CpFe(CO)(L)-C(O)R Type Organoiron Complexes and the Molecular Structure of *trans*-CpFe(H)(CO)(SnPh₃)₂. *Organometallics* **1991**, *10*, 3080–3089.

(38) (a) Hamon, P.; Toupet, L.; Hamon, J. R.; Lapinte, C. Novel Diamagnetic and Paramagnetic Iron(II), Iron(III), and Iron(IV) Classical and Nonclassical Hydrides. X-ray Crystal Structure of $[\text{Fe}(\text{C}_5\text{Me}_5)(\text{dppe})\text{D}]\text{PF}_6$. *Organometallics* **1992**, *11*, 1429–1431. (b) Yao, Z.; Klabunde, K. J.; Asirvatham, A. S. Unusual Iron(IV) Complexes: Metal Atom Syntheses and Studies of $(\eta^6\text{-arene})\text{Fe}(\text{H})_2(\text{SiCl}_3)_2$ (Arene = Benzene, Toluene, *p*-Xylene). *Inorg. Chem.* **1995**, *34*, 5289–5294. (c) Gusev, D. G.; Hübener, R.; Burger, P.; Orama, O.; Berke, H. Synthesis, Structural Diversity, Dynamics, and Acidity of the M(II) and M(IV) Complexes $[\text{MH}_3(\text{PR}_3)_4]^+$ (M = Fe, Ru, Os; R = Me, Et). *J. Am. Chem. Soc.* **1997**, *119*, 3716–3731. (d) Daida, E. J.; Peters, J. C. Considering $\text{Fe}^{\text{II/IV}}$ Redox Processes as Mechanistically Relevant to the Catalytic Hydrogenation of Olefins by $[\text{PhB}(\text{P}i\text{Pr}_3)_3]\text{Fe-H}_x$ Species. *Inorg. Chem.* **2004**, *43*, 7474–7485.

(39) (a) Maity, A.; Teets, T. S. Main Group Lewis Acid-Mediated Transformations of Transition-Metal Hydride Complexes. *Chem. Rev.* **2016**, *116*, 8873–8911. (b) Corey, J. Y. Reactions of Hydrosilanes with Transition Metal Complexes. *Chem. Rev.* **2016**, *116*, 11291–11435. (c) Liu, Y.; Su, B.; Dong, W.; Li, Z. H.; Wang, H. Structural Characterization of a Boron(III) $\eta^2\text{-}\sigma$ -Silane-Complex. *J. Am. Chem. Soc.* **2019**, *141*, 8358–8363.

(40) (a) Schubert, U.; Kunz, E.; Harkers, B.; Willnecker, J.; Meyer, J. η^2 -Coordination of a Sn-H Bond to a Transition Metal. Molecular Structure of $(\eta^2\text{-MeC}_5\text{H}_4)(\text{CO})_2\text{Mn}(\text{H})\text{SnPh}_3$. *J. Am. Chem. Soc.* **1989**, *111*, 2572–2574. (b) Carlton, L. Rhodium-Hydrogen-Tin Three-Center Bonds. NMR (^1H , ^{31}P , ^{103}Rh , ^{119}Sn) Study of $[\text{Rh}(\text{Cl})(\text{H})(\text{SnPh}_3)(\text{PPh}_3)(\text{py})]$ and Related Compounds. *Inorg. Chem.* **2000**, *39*, 4510–4519. (c) Carlton, L.; Fernandes, M. A.; Sitabule, E. An NMR Study of *trans* Ligand Influence in Rhodium η^2 -Triphenyltin Hydride Complexes. *Proc. Natl. Acad. Sci. U. S. A.* **2007**, *104*, 6969–6973.

(41) Forster, F.; Rendón López, V. M.; Oestreich, M. Z-Selective Hydrostannylation of Terminal and Internal C–C Triple Bonds Initiated by the Trityl Cation. *Organometallics* **2018**, *37*, 2656–2659.

(42) Liang, Q.; Song, D. Iron N-Heterocyclic Carbene Complexes in Homogeneous Catalysis. *Chem. Soc. Rev.* **2020**, *49*, 1209–1232.

(43) (a) Bruce, M. I. Organometallic Chemistry of Vinylidene and Related Unsaturated Carbenes. *Chem. Rev.* **1991**, *91*, 197–257. (b) Roh, S. W.; Choi, K.; Lee, C. Transition Metal Vinylidene- and Allenylidene-Mediated Catalysis in Organic Synthesis. *Chem. Rev.* **2019**, *119*, 4293–4356. (c) Chen, D.; Hua, Y.; Xia, H. Metal-*la*aromatic Chemistry: History and Development. *Chem. Rev.* **2020**, *120*, 12994–13086.

(44) Arndt, M.; Salih, K.; Fromm, A.; Goossen, L.; Menges, F.; Niedner-Schatteburg, G. Mechanistic Investigation of the Ru-Catalyzed Hydroamidation of Terminal Alkynes. *J. Am. Chem. Soc.* **2011**, *133*, 7428–7449.

(45) (a) Davison, A.; Selegue, J. Stable Dimethyl, Methyl, and Unsubstituted Vinylidene Complexes. *J. Am. Chem. Soc.* **1978**, *100*, 7763–7765. (b) Selegue, J. P. Electrophilic Attack on a Metal Alkynyl by Carbon Disulfide: Preparation and Structure of $[\text{Fe}(\text{C}_2\text{MeCS}_2\text{Me})(\text{dppe})(\text{Cp})]\text{I MeOH}$, a Cationic Vinylidene Complex. *J. Am. Chem. Soc.* **1982**, *104*, 119–124. (c) Consiglio, G.; Bangerter, F.; Darpin, C.; Morandini, F.; Lucchini, V. Diastereomeric Equilibria and Barrier of Rotation in Cationic Iron Diphosphine Alkylidene Carbene (Vinylidene) Complexes. *Organometallics* **1984**, *3*, 1446–1448.

(46) Liang, H.; Ji, Y.; Wang, R.; Zhang, Z.; Zhang, B. Visible-Light-Initiated Manganese-Catalyzed *E*-Selective Hydrosilylation and Hydrogermylation of Alkynes. *Org. Lett.* **2019**, *21*, 2750–2754.

(47) (a) Song, L.; Feng, Q.; Wang, Y.; Ding, S.; Wu, Y.; Zhang, X.; Chung, L. W.; Sun, J. Ru-Catalyzed Migratory Geminal Semihydrogenation of Internal Alkynes to Terminal Olefins. *J. Am. Chem. Soc.* **2019**, *141*, 17441–17451. (b) Feng, Q.; Wu, H.; Li, X.; Song, L.; Chung, L. W.; Wu, Y.; Sun, J. Ru-Catalyzed Geminal Hydroboration of Silyl Alkynes via a New *gem*-Addition Mechanism. *J. Am. Chem. Soc.* **2020**, *142*, 13867–13877.